

NHS Breast Screening Programme Equipment Report: Technical Evaluation of Siemens MAMMOMAT B.brilliant digital mammography system in 2D mode

December 2024



Contents

Executive Summary	4
Background	5
Disclaimer	5
1. Introduction	7
1.1 Testing procedures and performance standards for digital mammography	7
1.2 Objectives	7
2. Methods	8
2.1 System tested	8
2.2 Image processing	10
2.3 Output and HVL	10
2.4 Detector response	10
2.5 Dose estimation	10
2.6 Contrast-to-noise ratio	11
2.7 AEC performance for local dense areas	13
2.8 Noise analysis	14
2.9 Image quality measurements	15
2.10 Physical measurements of the detector performance	18
2.11 Other tests	18
3. Results	18
3.1 Output and HVL	18
3.2 Detector response	19
3.3 AEC performance	19
3.3.1 Dose	19
3.3.2 Contrast-to-Noise ratio	21
3.3.3 AEC performance for local dense areas	23

3.4	Noise measurements	24
3.5	Image quality measurements	26
3.6	Detector performance	29
3.7	Other tests	32
3.7.1	Alignment	32
3.7.2	Image retention	32
3.7.3	AEC repeatability	32
3.7.4	Uniformity and artefacts	33
3.7.5	Cycle time	34
3.7.6	Backup timer	34
3.7.7	Focal spot	34
3.7.8	Mesh	34
4.	Discussion	35
4.1	Dose and contrast-to-noise ratio	35
4.2	Local dense area	35
4.3	Noise analysis	36
4.4	Image quality	36
4.5	Detector performance	36
4.6	Other tests	36
5.	Conclusions	36
	References	38

Please note: The image shown in Figure 1 is courtesy of Siemens.

Executive Summary

The technical performance of the Siemens MAMMOMAT B.brilliant was assessed in 2D mode.

The Dance mean glandular dose (MGD) was found to be well below the remedial level for all automatic exposure control (AEC) dose modes. For a 53mm equivalent standard breast, the Dance MGD was 0.99mGy, compared with the remedial level of 2.5mGy. The image quality, measured by threshold gold thickness using the CDMAM 3.4 test object, was at the achievable level.

Technical performance of this equipment operating in 2D mode was found to be satisfactory and the system could proceed to practical evaluation of 2D mode. The technical evaluation of the performance in tomosynthesis mode is published as a separate report.

Background

Mammographic equipment approved for use in the NHSBSP is subject to evaluation commissioned by NHS England and carried out by a number of breast screening services in England who undertake the practical evaluation of equipment using protocols provided by the NHSBSP. These evaluations comprise a staged process as follows:

1. A technical evaluation by the National Coordinating Centre for the Physics of Mammography (“NCCPM”) (the “Technical Evaluation”)
2. If the Technical Evaluation meets requirements, a subsequent practical evaluation is conducted by one of the breast screening services involved in the NHSBSP (the “Practical Evaluation”)

Technical and Practical Evaluations are undertaken to assess the use of equipment in a practical, clinical setting and are not intended to be clinical trials. Further information about the limitations of the Technical Evaluation and Practical Evaluations are set out below.

The purpose of the Technical and Practical Evaluations together are intended to:

- determine the suitability of the equipment for use within the NHSBSP
- assist potential purchasers in making their choice of equipment
- provide potential users with performance data about equipment
- provide potential users with a record of the practical experience of using the equipment in the NHSBSP
- enable comparisons to be made with other pieces of tested equipment.

Disclaimer

Whilst NHS England commissions testing for the purposes outlined above, in order to provide further information and support to providers of screening services within the NHSBSP, it is for informational purposes only and such testing is subject to the limitations described below. No representation is made by NHS England in relation to the reports generated from the Technical Evaluation or the Practical Evaluation and, insofar as the law allows, NHS England accepts no liability arising from purchase or use of equipment by providers of screening services within the NHSBSP subjected to them.

Providers of screening services within the NHSBSP must ensure that all equipment purchased and used within the NHSBSP complies with all relevant requirements of the NHSBSP, the terms of their contracts in respect of the NHSBSP, and all other relevant obligations including but not limited to ensuring that such equipment:

- complies with national equipment standards
- has been approved for use in the programme and is tested by appropriately trained staff and medical physics services, in accordance with NHSBSP guidelines
- is accredited for use within the NHSBSP and that image quality and radiation dose meet acceptable standards
- is suitable for the usage intended in the breast screening unit.

Providers are reminded that they should carry out their own due diligence in respect of the above.

Testing undertaken during the Technical Evaluation is a balance between time, evaluation costs and depth. There are therefore limitations to the scope of the Evaluations undertaken on the behalf of the NHSBSP.

The Technical Evaluation is undertaken over a short time and so will not assess if image quality may change over time. The equipment tested is generally selected by the equipment supplier and has been set up by them. It should be noted that individual centres may be set up differently for example to meet the requirements of the screening service.

The technical image quality as measured on this system must be acceptable. The image quality of the final displayed image will be affected by the image processing and display and this is separately evaluated qualitatively in the Practical Evaluation.

This evaluation report does not absolve the provider of their responsibility during the procurement process to ensure the equipment is suitable for the usage intended by the provider.

1. Introduction

1.1 Testing procedures and performance standards for digital mammography

This report is one of a series evaluating commercially available direct digital radiography (DR) systems for mammography on behalf of the NHS Breast Screening Programme (NHSBSP) [1] [2] [3] [4] [5]. The testing methods and standards applied are mainly derived from NHSBSP Equipment Report 0604 [6] which is referred to in this document as ‘the NHSBSP protocol’. The standards for image quality and dose are the same as those provided in the European protocol, [7] [8] but the latter has been followed where it provides a more detailed standard, for example, for the automatic exposure control (AEC) system.

Some additional tests were carried out according to the UK recommendations for testing mammography X-ray equipment as described in IPEM Report 89 [9].

1.2 Objectives

The aims of the evaluation were:

- to determine whether the Siemens MAMMOMAT B.brilliant digital mammography system, operating in 2D mode, meets the main standards in the NHSBSP and European protocols
- to provide performance data for comparison against other systems.

2. Methods

2.1 System tested

The tests were conducted at the Siemens factory in Forchheim, Germany on a Siemens MAMMOMAT B.brilliant system as described in Table 1. The MAMMOMAT B.brilliant is shown in Figure 1.

Table 1. System description

Manufacturer	Siemens Healthineers		
Model	MAMMOMAT B.brilliant		
System serial number	241		
Target material	Tungsten (W)		
Added filtration	1.0mm Aluminium (Al) for 2D, 0.7mm Al for tomosynthesis		
Detector type	Amorphous selenium		
Detector serial number	PROTO-0014		
Pixel pitch	85µm		
Detector size	304.64mm x 239.36mm		
Pixel array	2816 x 3584 (2812x3528 maximum active in 2D)		
Typical image sizes	14.3MB (201 mm x 269 mm field size) 18.9MB (239.0 mm x 299.9 mm field size)		
Source to detector distance	650mm		
Source to table distance	636mm		
Pre-exposure mAs	2D Low Energy / Tomosynthesis: Compression force <=30N: 4mAs 0-30mm: 3mAs 31-50mm: 4mAs 51-200mm: 5mAs	2D High Energy: 3mAs for all thicknesses	Magnification: Compression force <=30N: 3mAs 0-30mm: 2mAs 31-50mm: 3mAs 51-200mm: 4mAs
Automatic exposure control (AEC) modes	OPDOSE, segmentation on or off, five selectable dose levels: normal, -20%, -11%, +12%, +25% In addition to the selectable dose levels service engineers can configure relative dose levels either for the system as a whole or for specific CBT ranges. The default values on the system tested are shown in Tables 6 and 7.		
Software version	VA10C		

The system tested was equipped with the PRIME (Progressive Reconstruction Intelligently Minimising Exposure) option, which may be used for breast thicknesses up to 41mm. Instead of the system using a grid, the software identifies structures in the breast that cause scatter, and subtracts the estimated scatter signal. The system is able to select a lower mAs when PRIME is in operation, as the primary X-rays are not absorbed by a grid. The dose saving depends on breast thickness but may reduce image quality.

PRIME may be selected or deselected at the acquisition workstation. The AEC system has five dose settings: low, medium low, normal, medium high and high. These allow selection of dose levels of 80%, 89%, 100%, 112%, and 125% of the normal dose

OPDOSE uses the measured compressed breast thickness to pick the kVp for both the pre-exposure and the exposure itself and to pick the mAs for the pre-exposure.

The AEC is a “smart” system which identifies a denser region in the breast, a process known as segmentation. The system uses this denser region to select the appropriate exposure factors. If the tube is angled for an oblique view, a triangular region at the chest wall, corresponding to the expected position of pectoral muscle, is excluded from the search for a dense area.



Figure 1. The Siemens MAMMOMAT B.brilliant system

2.2 Image processing

The MAMMOMAT B.brilliant has several options for the image processing known as “flavors”, from 0 to 5 with the default being “Flavor 1” and the primary alternative being “Flavor 5”. There are additional configurations of the post processing possible to adapt the image impression to customer wishes. The settings include for example changes of image sharpness and image contrast.

2.3 Output and HVL

The output and half-value-layer (HVL) were measured as described in the NHSBSP protocol [6], at intervals of 3kV.

2.4 Detector response

The detector response was measured with 2mm aluminium at the tube head. The grid and paddle were removed and a dosimeter was positioned above the breast support, 50mm from the chest wall edge (CWE). The incident air kerma was measured for a range of manually set mAs values at 27kVp W/AI_{1.0mm} anode/filter combination. The readings were corrected to the surface of the detector using the inverse square law. No correction was made for attenuation by the detector housing. A 10mm x 10mm region of interest (ROI) was positioned on the midline, 50mm from the CWE of each image. The average pixel value and the standard deviation of pixel values within the ROI were measured. The relationship between average pixel values and the incident air kerma to the detector was determined.

2.5 Dose estimation

Doses were measured by exposing different thicknesses of PMMA under AEC with segmentation turned off. Each PMMA block had an area of 180mm x 240mm. Spacers were used to adjust the paddle height to be equal to the equivalent breast thickness, as shown in Table 3. The exposure factors were noted and mean glandular doses (MGDs) were calculated for breasts of equivalent thicknesses using the Dance dosimetry model [10] [11] [12].

For 2D exposures the MAMMOMAT B.brilliant uses a 1.0mm thick Aluminium (Al) filter. This is not explicitly present in the published Dance [10] [11] [12] data, however the Dance model includes corrections for a wide range of HVLs which were achieved using additional aluminium filtration in the monte carlo simulations. In effect the Dance method already

corrects for different thicknesses of aluminium filtration and the existing AI factors can be used for the MAMMOMAT B.brilliant.

Although not yet adopted in UK breast screening programmes, a joint AAPM TG282 and EFOMP report on breast dosimetry was published recently [13]. The model proposed in this collaboration is intended by the authors as a future international standard. Mean glandular doses were therefore also estimated and tabulated using the TG282 model for cranio-caudal (CC) views applying TG282 median percentile glandularities.

An aluminium square, 10mm x 10mm and 0.2mm thick, was used with the PMMA during these exposures, so that the images produced could be used for the calculation of the contrast-to-noise ratio (CNR), described in Section 2.6. The aluminium square was placed between two 10mm thick slabs of 180mm x 240mm PMMA, on the midline, with its centre 60mm from the CWE. Additional layers of PMMA were placed on top to vary the total thickness.

2.6 Contrast-to-noise ratio

Unprocessed images acquired during the dose measurement were analysed to obtain the CNRs. Thirty six small square ROIs (approximately 2.5mm x 2.5mm) were used to determine the average signal and the standard deviation in the signal within the image of the aluminium square (4 ROIs) and the surrounding background (32 ROIs), as shown in Figure 2. Small ROIs are used to minimise distortions due to the heel effect and other causes of non-uniformity [14]. The CNR was calculated for each image, as defined in the NHSBSP and European Protocols.

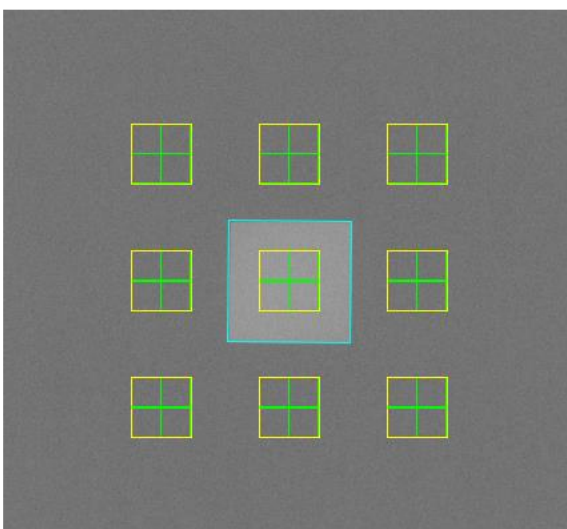


Figure 2: Location and size of ROI used to determine the CNR

To apply the standards in the European protocol, it is necessary to relate the image quality measured using the CDMAM (Section 2.9) for an equivalent breast thickness of 60mm, to that for other breast thicknesses. The European protocol [8] gives the relationship between threshold contrast and CNR measurements, enabling the calculation of a target CNR value for a particular level of image quality. This can be compared to CNR measurements made at other breast thicknesses. Contrast for a particular gold thickness is calculated using Equation 1, and target CNR is calculated using Equation 2.

$$\text{Contrast} = 1 - e^{-\mu t} \quad (1)$$

where μ is the effective attenuation coefficient for gold, and t is the gold thickness.

$$\text{CNR}_{\text{target}} = \frac{\text{CNR}_{\text{measured}} \times \text{TC}_{\text{measured}}}{\text{TC}_{\text{target}}} \quad (2)$$

where $\text{CNR}_{\text{measured}}$ is the CNR for a 60mm equivalent breast, $\text{TC}_{\text{measured}}$ is the threshold contrast calculated using the threshold gold thickness for a 0.1mm diameter detail, (measured using the CDMAM at the same dose as used for $\text{CNR}_{\text{measured}}$), and $\text{TC}_{\text{target}}$ is the calculated threshold contrast corresponding to the threshold gold thickness required to meet either the minimum acceptable or achievable level of image quality as defined in the NHSBSP protocol.

The threshold gold thickness for the 0.1mm diameter detail is used here because it is generally regarded as the most critical of the detail diameters for which performance standards are set.

The effective attenuation coefficient for gold used in Equation 1 depends on the beam quality used for the exposure, and the value used is in Table 2. This value was calculated with 3mm PMMA representing the compression paddle, using spectra from Hernandez et al [15] and attenuation coefficients for materials in the test objects (aluminium, gold, PMMA) from Berger et al [16].

The European protocol also defines a limiting value for CNR, which is calculated as a percentage of the threshold contrast for minimum acceptable image quality for each thickness. This limiting value varies with thickness, as shown in Table 3.

Table 2. Effective attenuation coefficient for gold contrast details in the CDMAM

kVp	Target/filter	Effective attenuation coefficient (μm^{-1})
27	W/1.0mm Al	0.1147

Table 3. Limiting values for relative CNR

Thickness of PMMA (mm)	Equivalent breast thickness (mm)	Limiting values for relative CNR (%) in European protocol
20	21	> 115
30	32	> 110
40	45	> 105
45	53	> 103
50	60	> 100
60	75	> 95
70	90	> 90

The target CNR values for minimum acceptable and achievable levels of image quality and European limiting values for CNR were calculated. These were compared with the measured CNR results for all breast thicknesses.

2.7 AEC performance for local dense areas

This test is described in the supplement to the fourth edition of the European protocol [8]. To simulate local dense areas, images of a 40mm thick block of PMMA of size 180mm x 240mm, were acquired under AEC. Extra pieces of PMMA between 2 and 14mm thick and of size 20mm x 40mm were added to provide extra attenuation. The compression plate remained in position at a height of 50mm, as shown in Figure 3. The simulated dense area was positioned 50mm from the CWE of the breast support table. The dimensions were chosen to match the tomosynthesis value set out in the EUREF report [17].

In the simulated local dense area the mean pixel value and standard deviation for a 10mm x 10mm ROI were measured and the signal-to-noise ratios (SNRs) were calculated. Thirty repeat measurements were made on the images varying the position of the ROI randomly (within the region covered by the extra PMMA) in order to obtain an estimate of uncertainty.

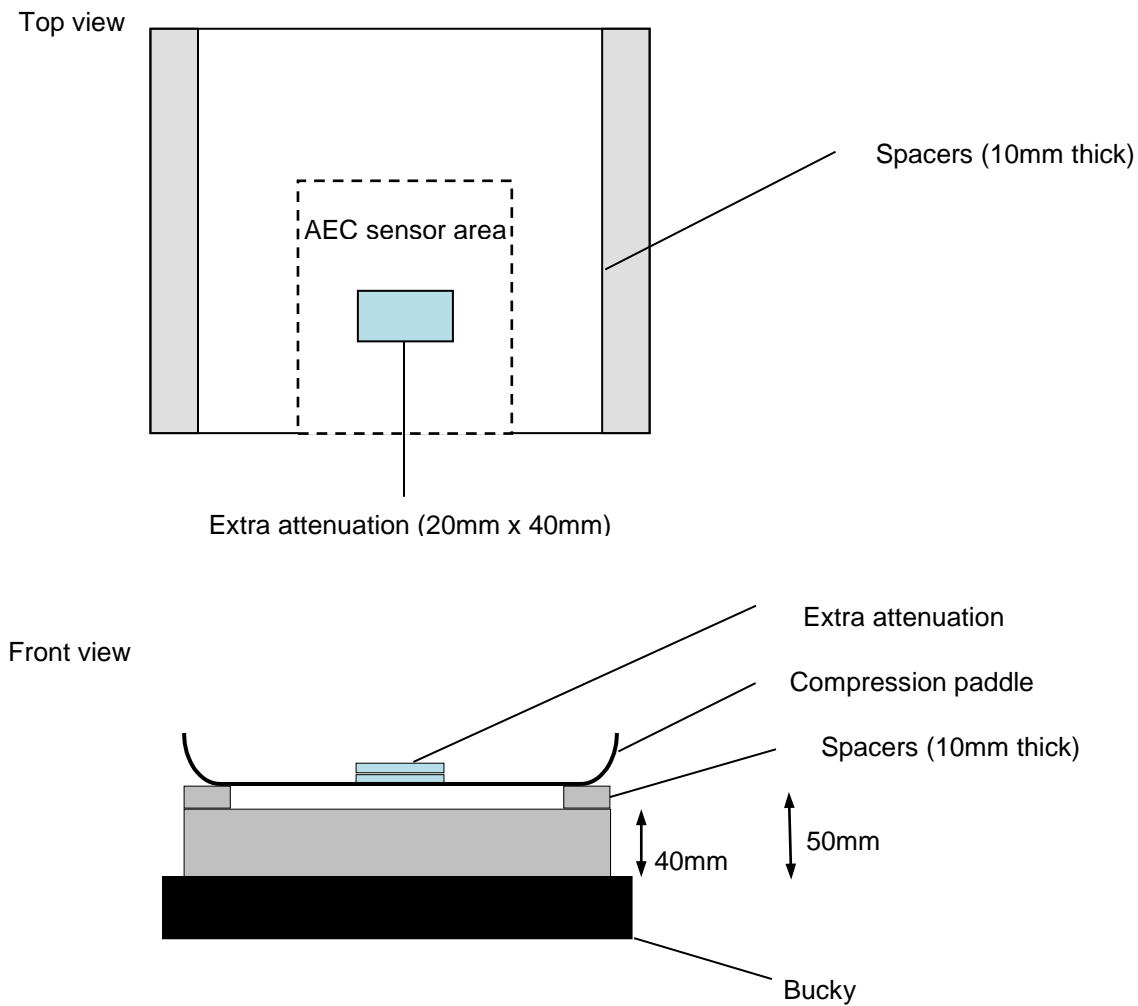


Figure 1. Setup to measure AEC performance for local dense areas

2.8 Noise analysis

The images acquired in the measurements of detector response, using 27kVp W/Al1.0mm, were used to analyse the image noise. Small ROIs with an area of approximately 2.5mm x 2.5mm were placed on the midline, 50mm from the CWE. The average of the standard deviations of the pixel values in each of the ROIs for each image were used to investigate the relationship between the air kerma incident to the detector and the image noise. A power fit of standard deviation against incident air kerma was made. If electronic and structure noise are small then a square root relationship is expected. It was assumed that the noise in the image comprises three components: electronic noise, structural noise, and quantum noise. The relationship between them is shown in Equation 3:

$$\sigma_p = \sqrt{k_e^2 + k_q^2 p + k_s^2 p^2} \quad (3)$$

where σ_p is the standard deviation in pixel values within an ROI with a uniform exposure and a mean pixel value p , and k_e , k_q , and k_s are the coefficients determining the amount of electronic, quantum, and structural noise in a pixel with a value p . This method of analysis has been described previously [18]. For simplicity, the noise is generally presented here as relative noise defined as in Equation 4.

$$\text{Relative noise} = \sigma_p / p \quad (4)$$

The variation in relative noise with mean pixel value was evaluated and fitted using Equation 3, and non-linear regression used to determine the best fit for the constants and their asymptotic confidence limits (using Graphpad Prism version 7.00 for Windows, Graphpad software, San Diego, California, USA, www.graphpad.com). This established whether the experimental measurements of the noise fitted this equation, and the relative proportions of the different noise components. The relationship between noise and pixel values has been found empirically to be approximated by a simple power relationship as shown in Equation 5.

$$\sigma_p / p = k_t p^{-n} \quad (5)$$

where k_t is a constant. If the noise were purely quantum noise the value of n would be 0.5. However the presence of electronic and structural noise means that n can be slightly higher or lower than 0.5. For graphical presentation in this report pixel values were converted to incident air kerma at the detector using the detector response data described in section 2.3.

The variance in pixel values within a ROI is defined as the standard deviation squared. The total variance against incident air kerma at the detector was fitted using Equation 3. Non-linear regression was used to determine the best fit for the constants and their asymptotic confidence limits, using the Graphpad Prism software.

Using the calculated constants, the structural, electronic, and quantum components of the variance were estimated, assuming that each component was independently related to incident air kerma. The percentage of the total variance represented by each component was then calculated and plotted against incident air kerma at the detector.

2.9 Image quality measurements

Contrast detail measurements were made using a CDMAM phantom (serial number 1022, version 3.4, UMC St. Radboud, Nijmegen University, Netherlands). The phantom was positioned with a 20mm thickness of PMMA above and below, to give a total attenuation

approximately equivalent to 50mm of PMMA or 60mm thickness of typical breast tissue. The exposure factors were chosen to match as closely as possible those selected by the AEC, at the standard dose setting, when imaging a 50mm thickness of PMMA. This procedure was repeated to obtain a representative sample of 16 images at this dose level. Further sets of 16 images of the test phantom were then obtained at other dose levels by manually selecting higher and lower mAs values with the same beam quality.

The CDMAM images were read and analysed automatically using Version 1.6 of CDCOM [19] [20]. and Version 2.1.0 of CDMAM Analysis (<https://medphys.royalsurrey.nhs.uk/nccpm/>). The threshold gold thickness for a typical human observer was predicted using Equation 6.

$$TC_{\text{predicted}} = rTC_{\text{auto}} \quad (6)$$

where $TC_{\text{predicted}}$ is the predicted threshold contrast for a typical observer, TC_{auto} is the threshold contrast measured using an automated procedure with CDMAM images. r is the average ratio between human and automatic threshold contrast determined experimentally with the values shown in Table 4.

The process was repeated using a CDMAM 4.0 phantom (serial number 4306, version 4.0, UMC St. Radboud, Nijmegen University, Netherlands).

Table 4. Values of r used to predict threshold contrast

Diameter of gold disc (mm)	Average ratio of human to automatically measured threshold contrast (r)
0.08	1.40
0.10	1.50
0.13	1.60
0.16	1.68
0.20	1.75
0.25	1.82
0.31	1.88
0.40	1.94
0.50	1.98
0.63	2.01
0.80	2.06
1.00	2.11

The predicted threshold gold thickness for each detail diameter in the range 0.1mm to 1.0mm was fitted with a curve for each dose level, using the relationship shown in Equation 7.

$$\text{Threshold gold thickness} = a + bx^{-1} + cx^{-2} + dx^{-3} \quad (7)$$

where x is the detail diameter, and a, b, c and d are coefficients adjusted to obtain a least squares fit.

The confidence limits for the predicted threshold gold thicknesses have been previously determined by a sampling method using a large set of images. The threshold contrasts quoted in the tables of results are derived from the fitted curves.

The expected relationship between threshold contrast and MGD is shown in Equation 8.

$$\text{Threshold contrast} = \lambda D^{-n} \quad (8)$$

where D is the MGD for a 60mm thick standard breast (equivalent to the test phantom configuration used for the image quality measurement), and λ is a constant to be fitted.

It is assumed that a similar equation applies when using threshold gold thickness instead of contrast. This equation was plotted with the experimental data for detail diameters of 0.1 and

0.25mm. The value of n resulting in the best fit to the experimental data was determined, and the doses required for target CNR values were calculated for data relating to these detail diameters.

The MGDs to reach the minimum and achievable image quality standards in the NHSBSP protocol were then estimated. The error in estimating these doses depends on the accuracy of the curve fitting procedure, and pooled data for several systems has been used to estimate 95% confidence limits of about 20%.

2.10 Physical measurements of the detector performance

The modulation transfer function (MTF), normalised noise power spectrum (NNPS) and the detective quantum efficiency (DQE) of the system were measured. The methods used were as close as possible to those described by the International Electrotechnical Commission (IEC) [21]. The radiation quality used for the measurements was adjusted by placing a uniform 2mm thick aluminium filter at the tube housing. The beam quality used was 27kVp W/AI1.0mm. The test device to measure the MTF comprised a 100mm x 80mm rectangle of stainless steel with a polished straight edge, of thickness 2mm. This test device was placed directly on the breast support table, and the grid was removed. The test device was positioned to measure the MTF in two directions, first almost perpendicular to the CWE and then almost parallel to it.

To measure the noise power spectrum the test device was removed and exposures made for a range of incident air kerma at the surface of the table. The DQE is presented as the average of measurements in the directions perpendicular and parallel to the CWE.

2.11 Other tests

Other tests carried out included tests prescribed in IPEM Report 89 [9] for mammographic X-ray sets, as well as those in the NHSBSP protocol for digital mammographic systems. In addition to the five ROI method for uniformity described in these documents, uniformity was also assessed using a sliding ROI of size 2mm by 2mm.

3. Results

3.1 Output and HVL

The output and HVL measurements are shown in Table 5.

Table 5. Output and HVL

kVp	Target/filter	Output ($\mu\text{Gy/mAs}$ at 1m)	HVL (mm Al)
25	W/Al _{1.0mm}	9.7	0.54
28	W/Al _{1.0mm}	15.7	0.63
31	W/Al _{1.0mm}	22.1	0.72
34	W/Al _{1.0mm}	28.9	0.80
37	W/Al _{1.0mm}	36.0	0.88

3.2 Detector response

The detector response is shown in Figure 4.

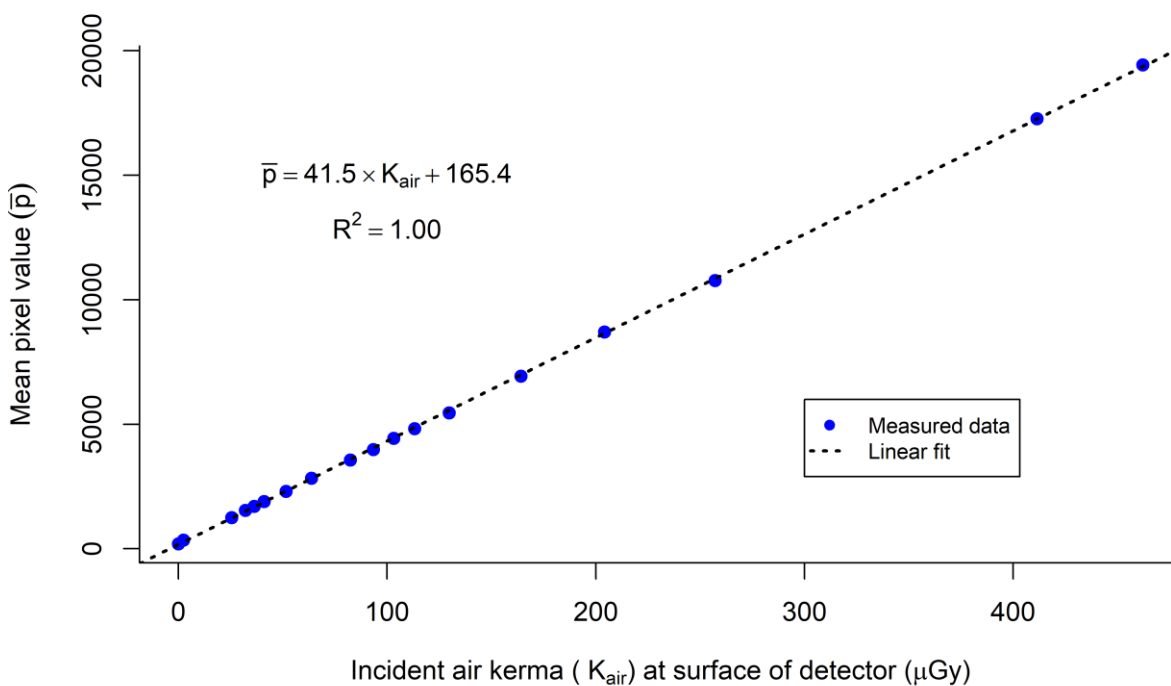


Figure 4. Detector response acquired at 27kVp W/Al1.0mm anode/filter combination with 2mm Al at the tube port

3.3 AEC performance

3.3.1 Dose

The MGDs for breasts simulated with PMMA exposed under AEC control are shown in Table 6 and Table 7 for exposures made in grid mode and with PRIME respectively. These results were acquired with segmentation off, which is appropriate for physics measurements of

uniform blocks. The mAs values include the pre-exposure. The MGDs were calculated from the total mAs, including the pre-exposure. The results presented in Table 6 and Table 7 are also presented graphically in Figure 5.

It is worth noting that the Siemens displayed values are estimated using the Boone method with constant 50% glandularity across all compressed breast thicknesses.

Table 6. MGD for simulated breasts (normal dose, grid in, segmentation off)

PMMA thickness (mm)	Equivalent breast thickness (mm)	AEC dose level	kVp	Target/filter	mAs	Dance MGD (mGy)	Remedial dose level (mGy)	Displayed dose (mGy)	TG282 MGD (mGy)
20	21	100%	25	W/Al _{1.0mm}	37.3	0.50	1.0	0.53	0.51
30	32	100%	26	W/Al _{1.0mm}	47.2	0.65	1.5	0.69	0.65
40	45	100%	26	W/Al _{1.0mm}	79.3	0.95	2.0	0.92	0.86
45	53	100%	27	W/Al _{1.0mm}	73.4	0.99	2.5	0.93	0.86
50	60	100%	27	W/Al _{1.0mm}	92.7	1.20	3.0	1.07	0.96
60	75	100%	28	W/Al _{1.0mm}	106.8	1.50	4.5	1.29	1.06
70	90	100%	30	W/Al _{1.0mm}	88.9	1.53	6.5	1.33	1.01
80	103	100%	31	W/Al _{1.0mm}	100.2	1.82	-	1.47	1.13

Table 7. MGD for simulated breasts (normal dose, PRIME, segmentation off)

PMMA thickness (mm)	Equivalent breast thickness (mm)	AEC dose level	kVp	Target/filter	mAs	Dance MGD (mGy)	Remedial dose level (mGy)	Displayed dose (mGy)	TG282 MGD (mGy)
20	21	82%	25	W/Al _{1.0mm}	31.5	0.42	1.0	0.45	0.43
30	32	90%	26	W/Al _{1.0mm}	44	0.61	1.5	0.64	0.61
40	45	100%	26	W/Al _{1.0mm}	79.3	0.95	2.0	0.92	0.86

Note: PRIME only operates for breast thicknesses up to 40mm.

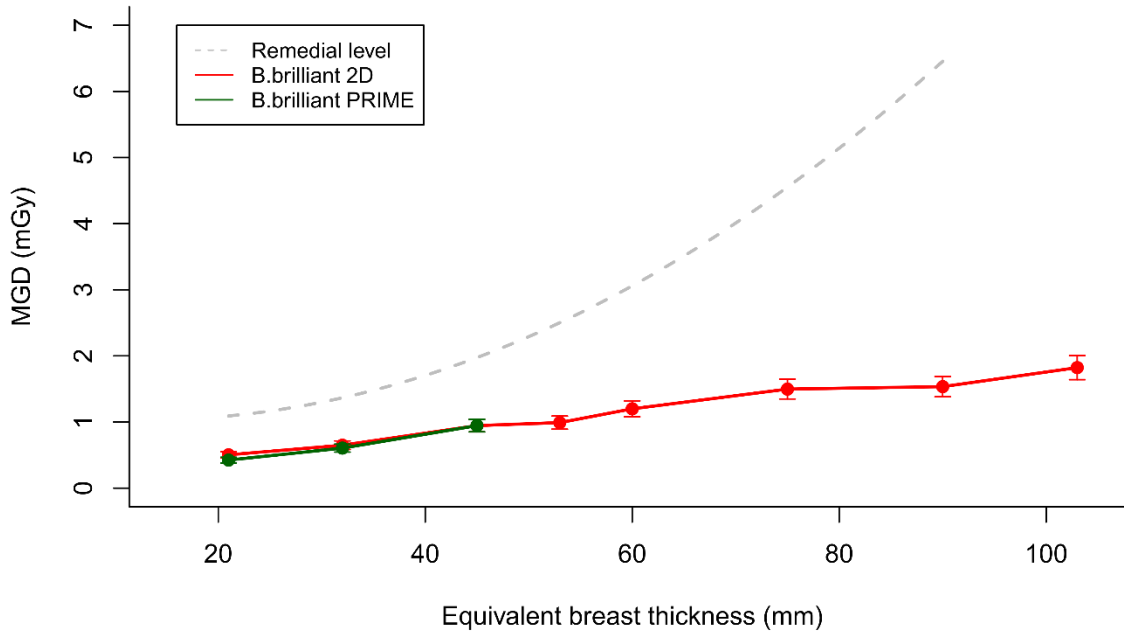


Figure 2. Dance MGD for different thicknesses of simulated breasts using AEC normal dose mode. (Error bars indicate 95% confidence limits)

3.3.2 Contrast-to-Noise ratio

The results of the CNR measurements for images acquired in grid mode and with PRIME are shown in Table 8 and Table 9 respectively and in Figure 6. The following calculated values are also shown:

- CNR to meet the minimum acceptable image quality standard
- CNR to meet the achievable image quality standard
- CNRs at each thickness to meet the limiting value in the European protocol

Table 8. CNR measurements (normal dose, grid in, segmentation off)

PMMA (mm)	Equivalent breast thickness (mm)	Measured CNR	CNR for minimum acceptable IQ	CNR for achievable IQ	European limiting CNR value
20	21	11.2	4.8	7.1	5.6
30	32	9.5	4.8	7.1	5.3
40	45	9.1	4.8	7.1	5.1
45	53	8.1	4.8	7.1	5.0
50	60	7.8	4.8	7.1	4.8
60	75	6.8	4.8	7.1	4.6
70	90	5.5	4.8	7.1	4.3
80	103	4.9	4.8	7.1	4.3

Table 9. CNR measurements (normal dose, PRIME, Segmentation off)

PMMA (mm)	Equivalent breast thickness (mm)	Measured CNR	CNR for minimum acceptable IQ	CNR for achievable IQ	European limiting CNR value
20	21	11.0	-	-	-
30	32	9.4	-	-	-
40	45	9.0	-	-	-

Note: PRIME only operates for breast thicknesses up to 40mm.

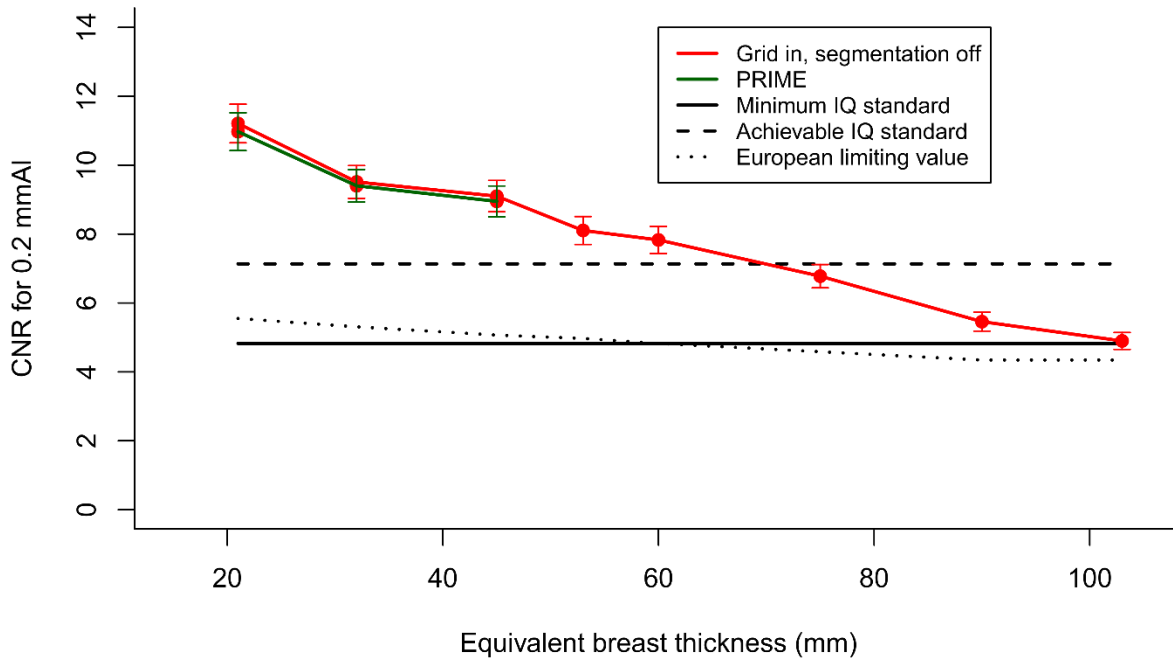


Figure 3. Measured CNR compared with the limiting values in the European protocol. (Error bars indicate 95% confidence limits.)

3.3.3 AEC performance for local dense areas

In grid mode (without PRIME) and with segmentation on, it is expected that when the AEC adjusts for local dense areas, the SNR remains constant with increasing thickness of extra PMMA. The results presented in Table 10 and Figure 7 show that the SNR does remain constant as thickness increases up to a total attenuation of 52mm PMMA. Above 52mm PMMA the mAs values selected by the AEC falls and a corresponding drop in the SNR was seen.

Table 10. AEC performance for local dense areas

Total attenuation (mm PMMA)	kVp	Target/filter	Tube load (mAs)	SNR	% SNR difference from mean SNR result
40	27	W/Al _{1.0mm}	66.1	72.5	10
42	27	W/Al _{1.0mm}	66.4	69.8	6
44	27	W/Al _{1.0mm}	69.9	67.6	3
46	27	W/Al _{1.0mm}	77.0	67.9	3
48	27	W/Al _{1.0mm}	81.4	66.6	1
50	27	W/Al _{1.0mm}	92.0	67.3	2
52	27	W/Al _{1.0mm}	92.0	64.2	-3
54	27	W/Al _{1.0mm}	67.5	51.4	-22

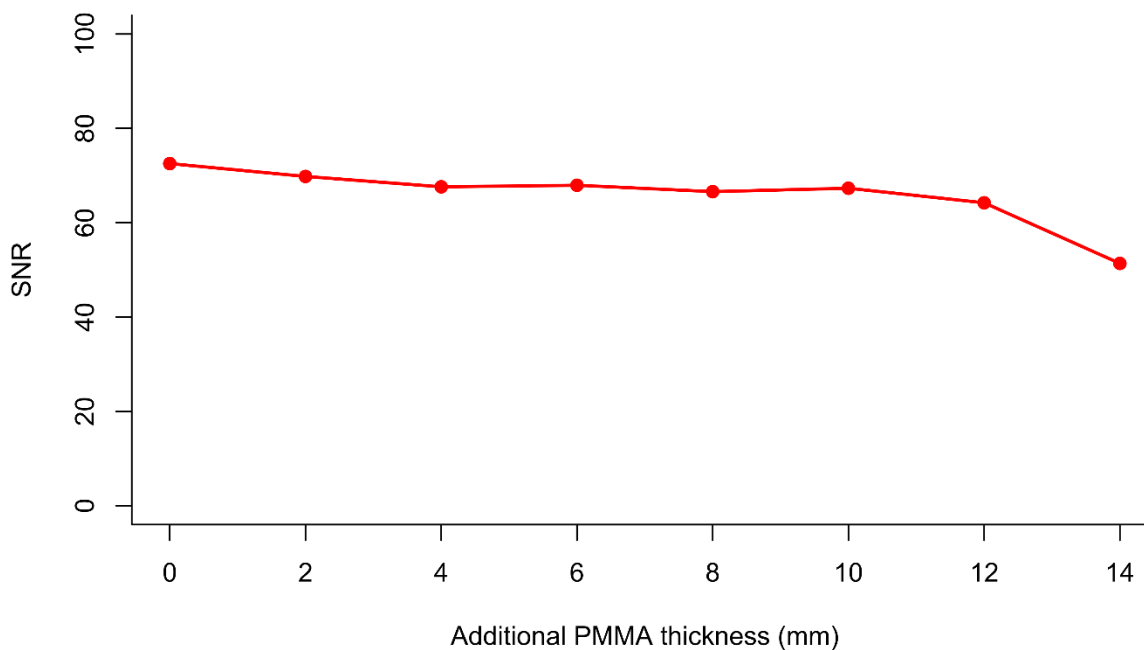


Figure 4. AEC performance for local dense areas

3.4 Noise measurements

The variation in noise with dose was analysed by plotting the standard deviation in pixel values against the incident air kerma to the detector, as shown in Figure 8. The fitted power curve has an index of 0.49, which is close to the expected value of 0.5 for quantum noise sources alone.

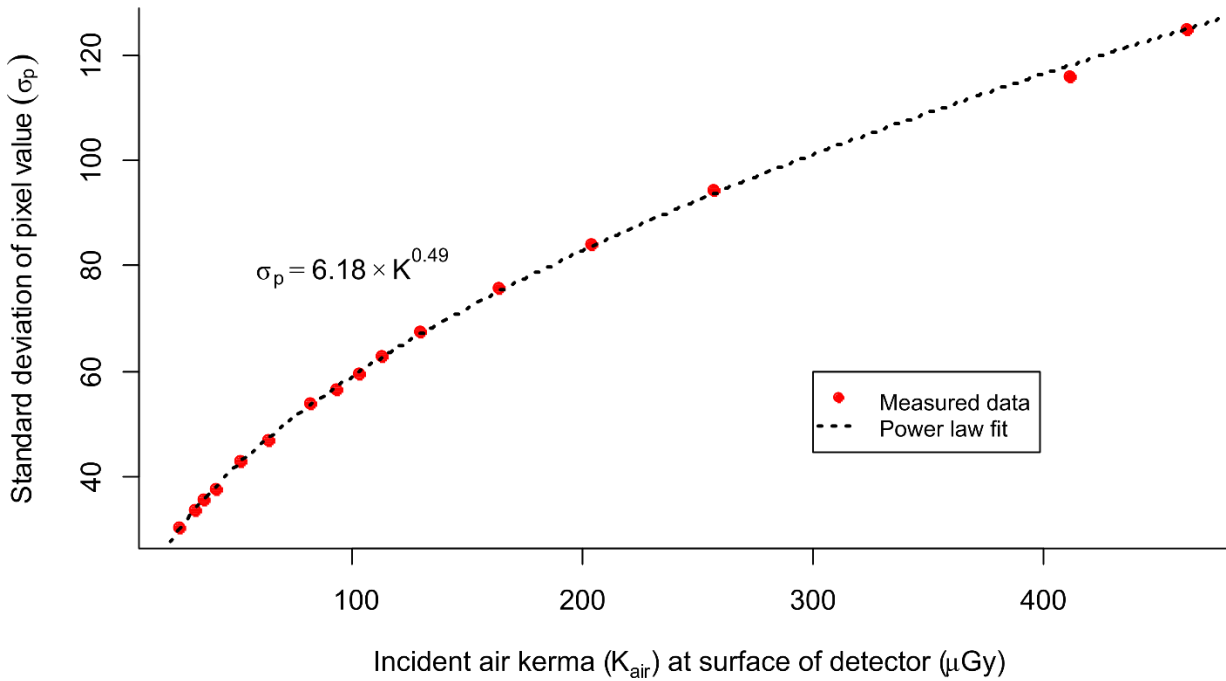


Figure 5. Standard deviation of linearized pixel values versus incident air kerma at detector

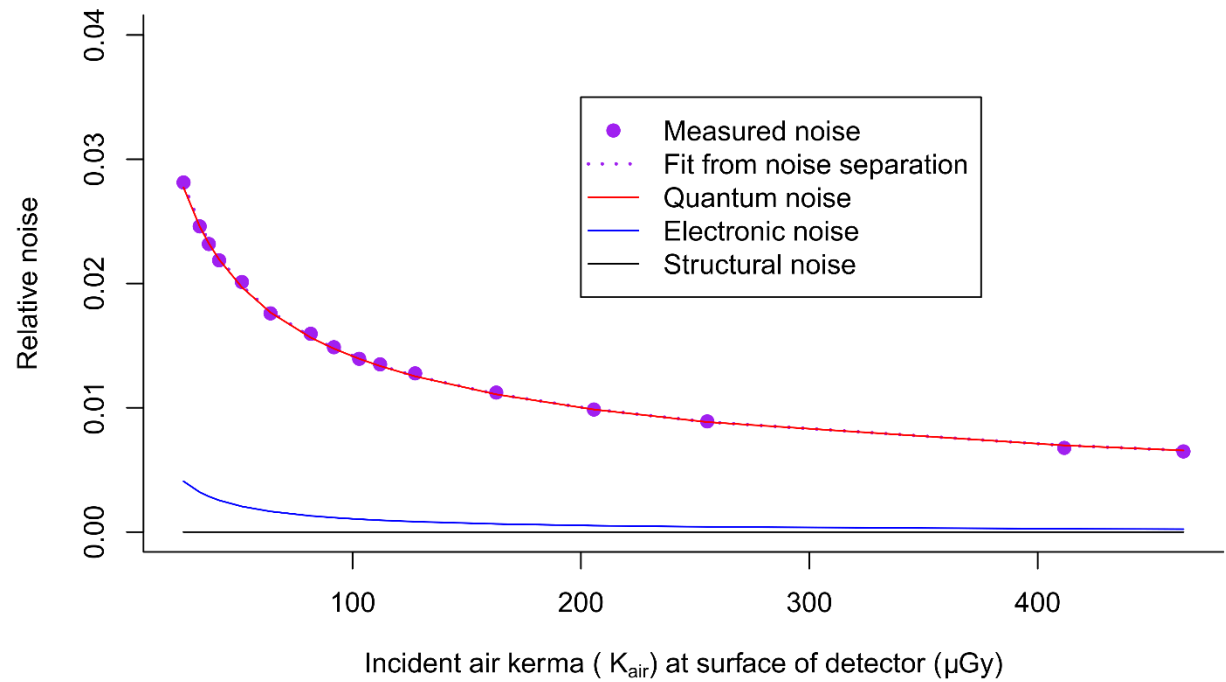


Figure 6. Relative noise and noise components

Figure 9 shows the relative noise at different incident air kerma. The estimated relative contributions of electronic, structural, and quantum noise are shown and the quadratic sum of these contributions fitted to the measured noise (using Equation 3).

Figure 10 shows the different amounts of variance due to each component. From this, the dose range over which the quantum component dominates can be seen.

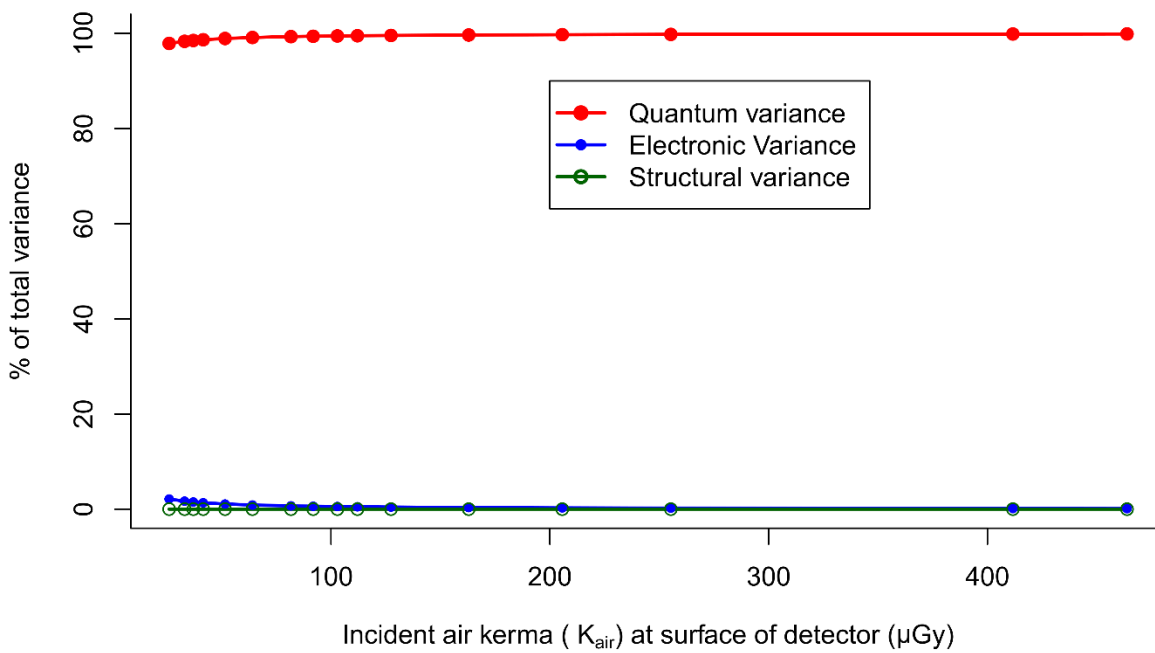


Figure 7. Noise components as a percentage of the total variance

3.5 Image quality measurements

The exposure factors used for each set of 16 CDMAM images are shown in Table 11. The Dance MGDs were chosen to cover a wide range centred around 1.16mGy, which was close to that selected for the equivalent breast of 60mm thick in AEC mode.

Table 11. Images acquired for image quality measurement

kVp	Target/filter	Tube loading (mAs)	Mean glandular dose to equivalent breasts 60mm thick (mGy)
27	W/AI _{1.0mm}	45.0 (0.5x AEC)	0.58
27	W/AI _{1.0mm}	63.0 (0.7x AEC)	0.82
27	W/AI _{1.0mm}	90.0 (1.0x AEC)	1.16
27	W/AI _{1.0mm}	140.0 (1.55x AEC)	1.81
27	W/AI _{1.0mm}	200.0 (2.2x AEC)	2.59

The contrast detail curves (determined by automatic reading of the images) at the different dose levels are shown in Figure 11. The threshold gold thicknesses measured for different detail diameters at the 5 selected dose levels are shown in Table 12. The NHSBSP minimum acceptable and achievable limits are also shown.

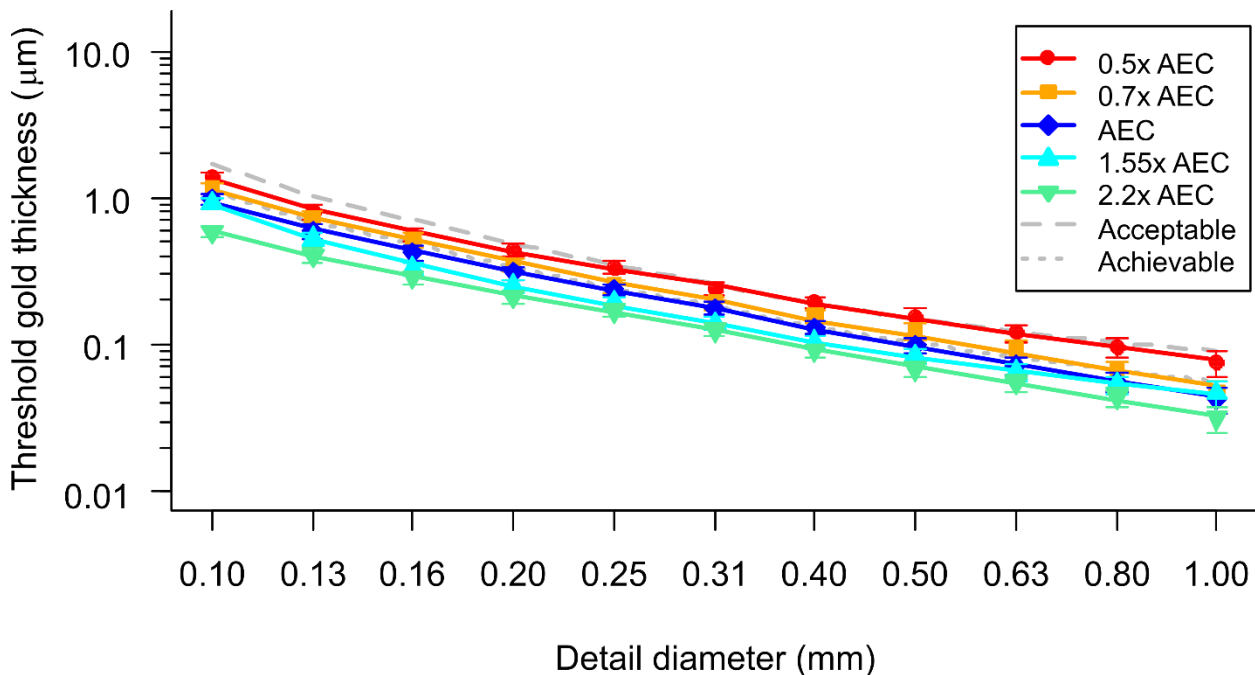


Figure 8. Threshold gold thickness detection curves for 5 doses at 27kV W/AI1.0mm. (Error bars indicate 95% confidence limits.) – CDMAM3.4

Table 12. Average threshold gold thicknesses for different detail diameters for 5 doses using 27kVp W/AI, and automatically predicted data – CDMAM 3.4

Diameter (mm)	Acceptable value	Achievable value	Threshold gold thickness (μm)				
			Mean Glandular Dose to equivalent breast 60mm thick (mGy)				
			0.58	0.82	1.16	1.81	2.59
0.1	1.680	1.100	1.33 ± 0.14	1.15 ± 0.11	0.94 ± 0.1	1.03 ± 0.09	0.59 ± 0.06
0.25	0.352	0.244	0.33 ± 0.03	0.27 ± 0.03	0.23 ± 0.02	0.28 ± 0.02	0.16 ± 0.02
0.5	0.150	0.103	0.15 ± 0.02	0.11 ± 0.01	0.1 ± 0.01	0.13 ± 0.01	0.07 ± 0.01
1	0.091	0.056	0.08 ± 0.02	0.05 ± 0.01	0.04 ± 0.01	0.07 ± 0.01	0.03 ± 0.01

The measured threshold gold thicknesses are plotted against the Dance MGD for an equivalent breast for the 0.1mm and 0.25mm detail sizes in Figure 13 from Table 12.

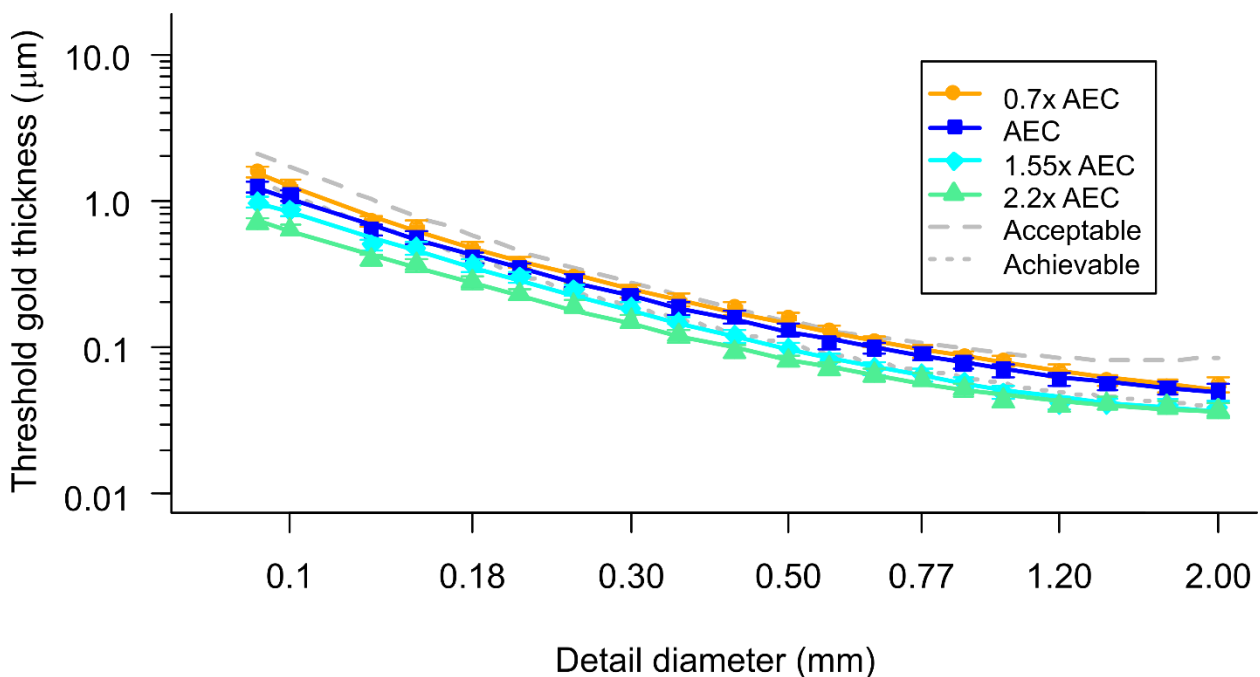


Figure 9. Threshold gold thickness detection curves for 4 doses at 27kV W/AI 1.0mm. (Error bars indicate 95% confidence limits) - CDMAM4.0

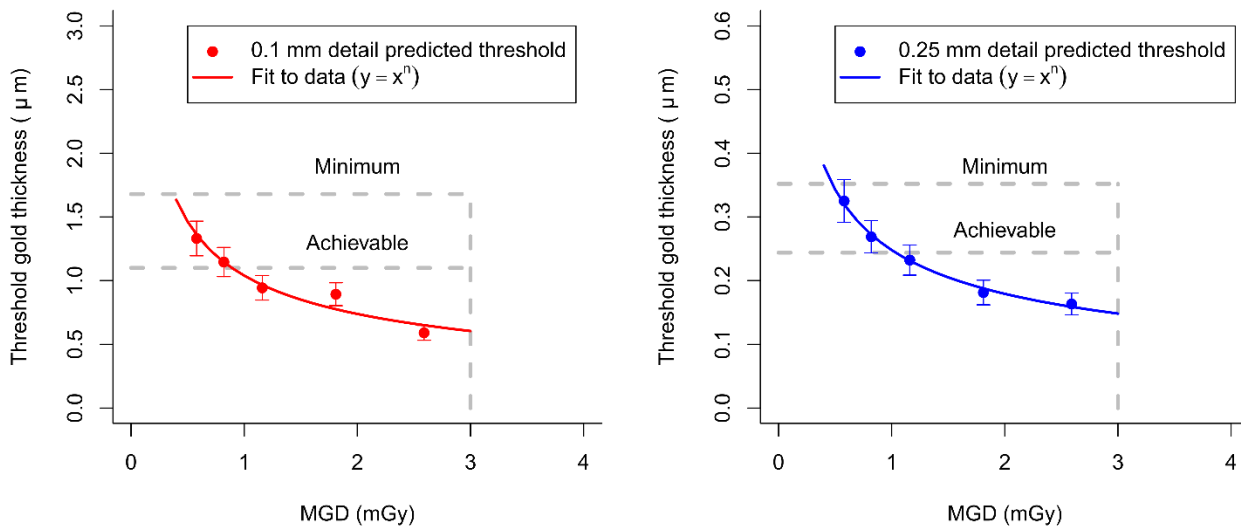


Figure 10. Threshold gold thickness at different doses. (Error bars indicate 95% confidence limits)

The Dance MGDs to reach the minimum and achievable image quality standards in the NHSBSP protocol for a 60mm equivalent breast thickness have been estimated from the curves shown in Figure 13. To reach the minimum threshold gold thickness Dance MGDs of $0.41 \pm 0.08\text{mGy}$ and $0.48 \pm 0.08\text{mGy}$ were required for 0.1 mm and 0.25mm details respectively. To reach the achievable threshold gold thickness Dance MGDs of $0.91 \pm 0.18\text{mGy}$ and $1.04 \pm 0.21\text{mGy}$ were required for 0.1mm and 0.25mm details respectively.

3.6 Detector performance

The MTF is shown in Figure 14 for the two orthogonal directions. Figure 15 shows the NNPS curves for a range of air kerma incident to the detector.

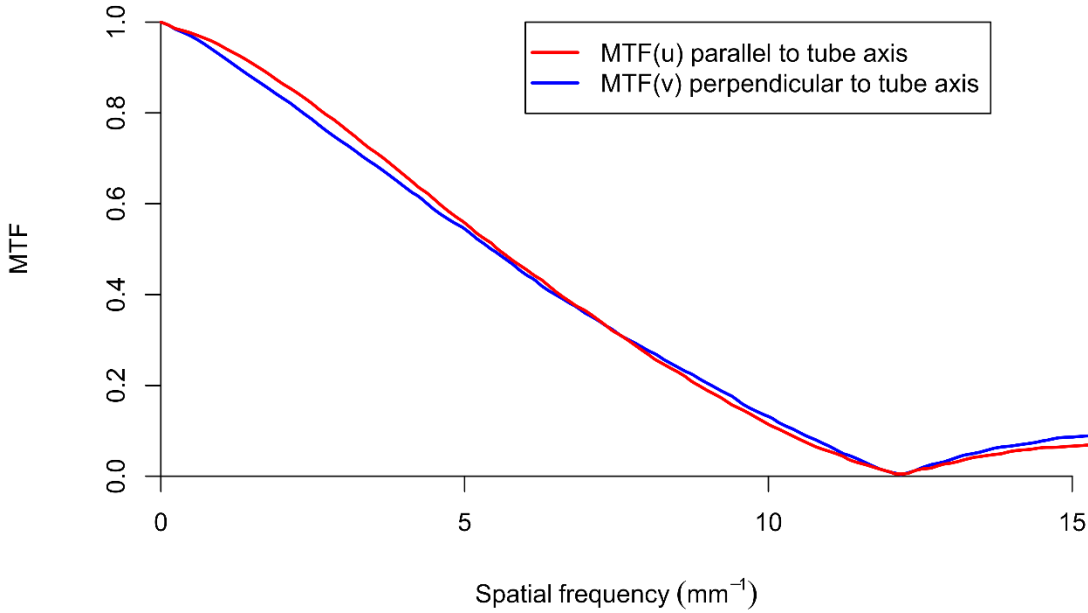


Figure 11. Pre-sampled MTF

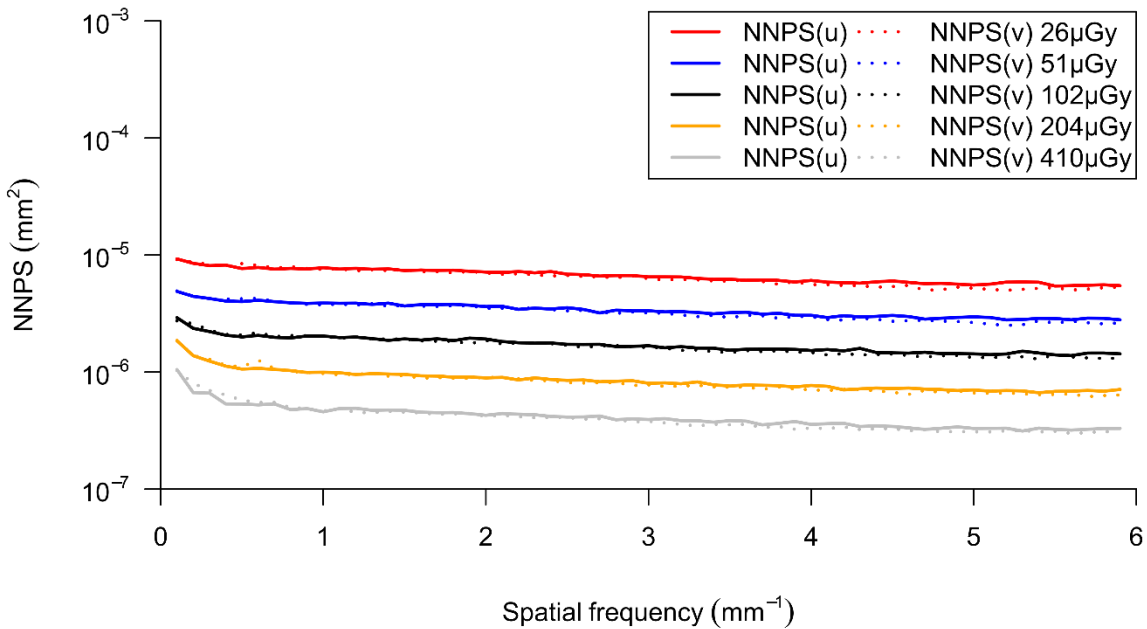


Figure 12. NNPS curves for a range of air kerma incident to the detector

Figure 16 shows the DQE averaged in two orthogonal directions for a range of incident air kerma. The spectra of Hernandez et al [15] were attenuated using the Bier-Lambert law with mass attenuation coefficients from Berger et al [16] and the mammographic filter thickness was adjusted iteratively until the calculated HVL matched the results in Table 5. The resulting spectra were used to estimate a q-factor of 5369 photons $\text{mm}^{-2} \mu\text{Gy}^{-1}$. The MTF and DQE measurements were interpolated to show values at standard frequencies in Table 13.

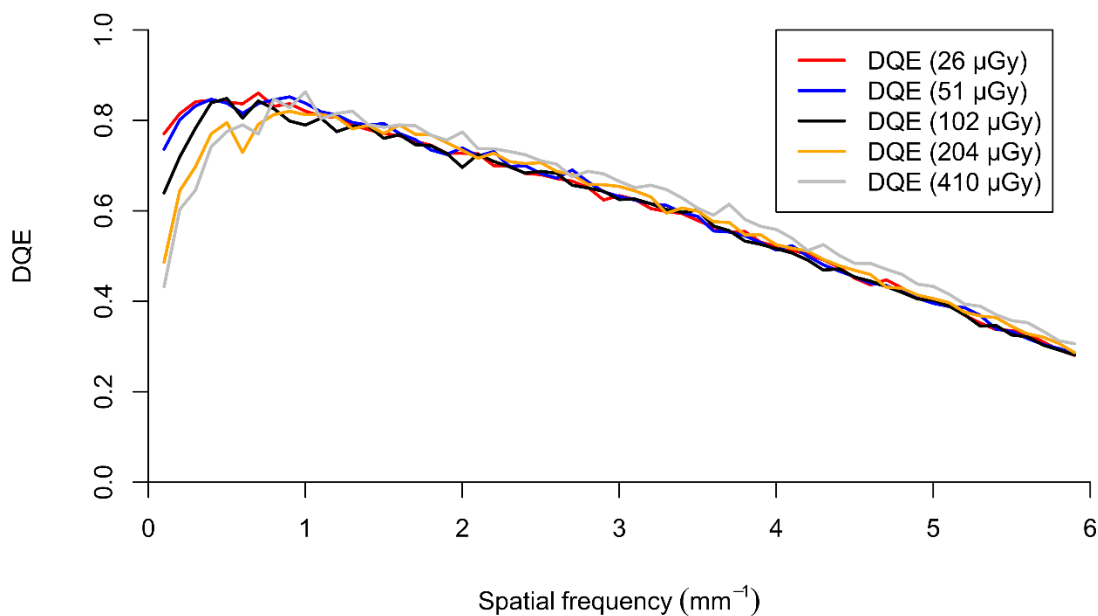


Figure 13. DQE averaged in both directions for a range of incident air kerma

Table 13. MTF and DQE measurements at standard frequencies (DQE at incident air kerma of 102µGy)

Frequency (mm ⁻¹)	MTF (u)	MTF (v)	DQE
0.0	1.00	1.00	-
0.5	0.97	0.97	0.83
1.0	0.95	0.92	0.79
1.5	0.91	0.88	0.77
2.0	0.87	0.84	0.72
2.5	0.81	0.78	0.68
3.0	0.77	0.73	0.63
3.5	0.72	0.69	0.60
4.0	0.67	0.64	0.52
4.5	0.60	0.58	0.44
5.0	0.56	0.54	0.40
5.5	0.51	0.49	0.33
6.0	0.46	0.45	0.28

3.7 Other tests

The results of all the other tests that were carried out were within acceptable limits as prescribed in the NHSBSP protocol [6] and IPEM Report 89 [9].

3.7.1 Alignment

Alignment measurements showed that the light field edges were all within 5mm of the edges of the radiation field (IPEM remedial level > 5mm). The radiation field overlapped the edges of the image by up to 4mm (remedial level < 0mm or > 5mm).

3.7.2 Image retention

The image retention factor was 0.04, compared to the NHSBSP upper limit of 0.3.

3.7.3 AEC repeatability

For a series of 5 repeat images, acquired in quick succession, the maximum deviation of mAs from the mean was 0.51%. The maximum deviation in SNR from the mean was 0.55%. Eighteen images were acquired at intervals over the full four days of testing. Time points were chosen such that some repeats were in the morning before any other exposure whilst others were immediately after an intensive series of exposures or at the end of the day after a full day of use. The maximum deviation in mAs for these acquisitions was 1.7% - the

NHSBSP remedial level is 5%. The maximum deviation in SNR from the mean over the full four days was 1.65%.

3.7.4 Uniformity and artefacts

Uniformity images acquired with PMMA on the breast support in the beam showed a variation in pixel values of 5.6% relative to the central area. The NHSBSP remedial level is 10%. Uniformity images acquired with no PMMA in the beam showed a variation in pixel values of 3.2% relative to the central area. There were no obvious structures or unusual areas within the uniformity images.

With PMMA the sliding ROI method gave a maximum variation from the mean of 9.2% and a maximum variation from the centre of 11.3%. With no PMMA the method gave a maximum variation from the mean of 5.2% and a maximum variation from the centre of 6.4%. This reflects the higher sensitivity of the sliding ROI technique and the fact that Siemens perform flat-fielding calibrations with no PMMA in the beam. Figure 17 shows the beam profile as a surface plot for an image of the 40mm of PMMA. This shows that the largest non-uniformities are a result of the anode-heel effect.

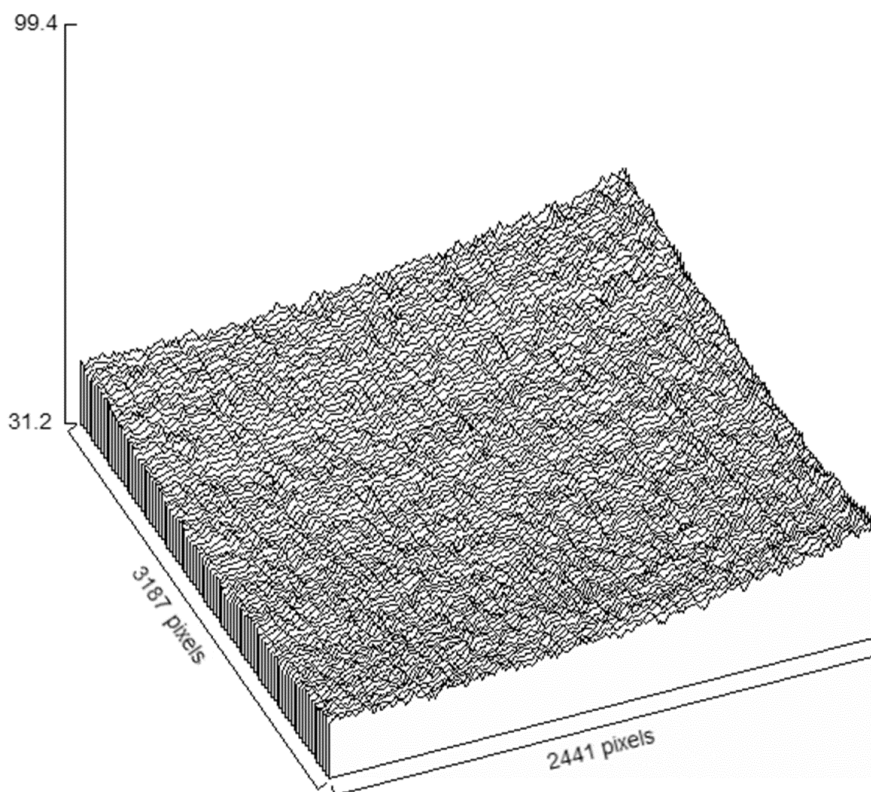


Figure 14. Beam profile of an image of 40mm PMMA under AEC

3.7.5 Cycle time

For a typical exposure of 45mm PMMA using 27kVp W/AI1.0mm and 73mAs, a subsequent exposure could be made 6 seconds after the start of the previous one.

3.7.6 Backup timer

When an AEC exposure was attempted with a steel plate blocking the X-ray beam the exposure terminated after the pre-exposure. There was no main exposure and no image acquired.

3.7.7 Focal spot

The measured dimensions of the broad focal spot were 0.28mm by 0.19mm - parallel and perpendicular to the chest wall edge respectively – compared to a nominal size of 0.3mm.

3.7.8 Mesh

No discontinuities or blurred regions were seen in the image of the mesh test object.

4. Discussion

4.1 Dose and contrast-to-noise ratio

The detector response was found to be a linear relationship with exposure. This was as expected for Siemens systems.

Dance MGDs measured using PMMA were well within the NHSBSP remedial dose levels for all equivalent breast thicknesses when using all AEC dose modes. In the normal AEC dose mode the Dance MGD to the 53mm thick standard breast model was 0.99mGy (Table 6).

CNR measurements made with plain PMMA showed an overall decrease in CNR with increased thickness of PMMA (Figure 6). Target CNR values of 4.8 and 7.1, for minimum acceptable and achievable image quality respectively, were calculated from the CNR and threshold gold thickness results.

In the normal dose AEC mode, the CNRs exceeded the target for the achievable level of image quality for equivalent breast thicknesses of up to 60mm. For higher equivalent breast thicknesses, the CNRs were below the achievable level but above the minimum.

In PRIME mode, MGDs to the standard breast model for equivalent breast thicknesses up to 40mm were 0% to 16% lower than the mode with the grid in. Correspondingly CNRs were measured to be approximately 2% lower. It should be noted that these results, measured with uniform blocks, will not necessarily directly relate to the performance of PRIME in clinical use. In clinical use, PRIME mode with segmentation on, works by identifying structures in the breast to both determine the exposure factors and to subtract the calculated scatter. Further information on PRIME and an explanation of how segmentation works is provided in NHSBSP Equipment Report 1503 [22]. It should be noted that the dose saving is smaller than that for the Siemens Revelation. Also, the maximum CBT for Prime is 40mm rather than 70mm used in the Revelation.

4.2 Local dense area

The local dense area test showed that with segmentation on the AEC identifies the presence of the dense area and increases the mAs in order to maintain SNR up to a total attenuation of 52mm of PMMA. For a total attenuation greater than 52mm the AEC excludes the dense area and the mAs dropped back to values close to those for 40mm PMMA and a drop in the SNR was seen corresponding to the fall in mAs. Siemens have confirmed that the system is performing as expected as an area of such high density is handled as non-natural material

inside the breast. By design of the software algorithm, this area is excluded from the analysis.

4.3 Noise analysis

Noise analysis showed that quantum noise dominates the noise over the whole range of incident air kermas that noise was measured (26 to 410 μ Gy) (Figure 10). The results show that there are minimal contributions from electronic and structural noise.

4.4 Image quality

Threshold gold thicknesses for a range of detail diameters are shown in Figure 11. At an MGD of 1.16mGy (close to that selected for the equivalent thickness of PMMA in Standard mode), the image quality was better than the achievable level for all contrast detail diameters.

Threshold gold thickness measurements at different dose levels for the 0.1mm and 0.25mm diameter details were used to calculate Dance MGDs to a 60mm equivalent breast required for the minimum and achievable levels of image quality (Figure 13).

4.5 Detector performance

The detector performance, as indicated by MTF, NNPS and DQE curves (Figures 14, 15 and 16), was provided for reference and was within expected results.

4.6 Other tests

The miscellaneous results presented under the section “Other tests” were satisfactory. As with the Siemens Revelation (VC20C and higher) flat-fielding is performed without a PMMA attenuator. The dominant sources of non-uniformity are likely to be the anode-heel effect and scatter distribution. The magnitude of the residual effect in an image is strongly dependent on the density and thickness of the breast (or in this case test object) being imaged. The flat-fielding process therefore doesn’t remove the need for a large-scale gradient correction as part of the image processing before clinical presentation. Measurements of uniformity performed with a PMMA attenuator largely reflect the differences in calibration and uniformity measurement conditions.

5. Conclusions

The technical performance of the Siemens MAMMOMAT B.brilliant in 2D mode was found to be satisfactory.



The Dance MGD to the 53mm thick standard breast in 2D mode was found to be 0.99mGy for the normal dose AEC mode. This is well below the remedial level. The image quality, as measured by threshold gold thickness, is at the achievable level.

References

- [1] A. Mackenzie and J. Oduko, "NHS Breast Screening Programme Equipment Report Technical Evaluation of Hologic 3Dimensions digital mammography system in 2D mode," Public Health England, London, 2019.
- [2] Public Health England, "NHS Breast Screening Programme Equipment Report: Technical evaluation of GE Senographe Pristina digital mammography system in 2D mode," Public Health England, London, 2019.
- [3] C. Strudley, A. Hadjipanteli, J. Oduko and K. Young, "NHS Breast Screening Programme Equipment Report: Technical evaluation of Fujifilm AMULET Innovality digital breast tomosynthesis system," Public Health England, London, 2018.
- [4] N. Tyler, K. Young, J. Oduko and A. Mackenzie, "NHS Breast Screening Programme Equipment Report: Technical Evaluation of IMS Giotto Class digital mammography system in 2D mode," Public Health England, London, 2019.
- [5] N. Tyler and A. Mackenzie, "NHS Breast Screening Programme Equipment Report: Technical Evaluation of Siemens Revelation digital mammography system in 2D mode," Public Health England, London, 2019.
- [6] E. Kulama, A. Burch, I. Castellano, C. P. Lawinski, N. Marshall and K. C. Young, "Commissioning and routine testing of full field digital mammography systems," NHS Cancer Screening Programmes, Sheffield, 2009.
- [7] R. van Engen, S. van Woudenberg, H. Bosmans, Y. KC and M. Thijssen, "European guidelines for quality assurance in breast cancer screening and diagnosis (4th edition): European protocol for the quality control of physical and technical aspects of mammography screening," European Commission, Luxembourg, 2006.
- [8] N. Perry, M. Broeders, C. de Wolf, S. Tornberg, R. Holland and L. von Karsa, "European guidelines for quality assurance in breast screening and diagnosis (4th Edition Supplements)," European Commission, Luxembourg, 2013.
- [9] A. C. Moore, D. R. Dance, D. S. Evans, C. P. Lawinski, E. M. Pitcher and A. Rust, "The commissioning and routine testing of mammographic X-ray systems," IPEM report 89, Institute of Physics and Engineering in Medicine, York, 2005.

- [10] D. R. Dance, "Monte Carlo calculation of conversion factors for the estimation of mean glandular breast dose," *Physics in Medicine and Biology*, vol. 35, pp. 1211-19, 1990.
- [11] D. R. Dance, C. L. Skinner, K. C. Young, J. R. Beckett and J. C. Kotre, "Additional factors for the estimation of mean glandular breast dose using the UK mammography dosimetry protocol," *Physics in Medicine and Biology*, vol. 45, pp. 3225-40, 2000.
- [12] D. R. Dance, K. C. Young and R. E. van Engen, "Further factors for the estimation of mean glandular dose using the United Kingdom, European and IAEA dosimetry protocols," *Physics in Medicine and Biology*, vol. 54, pp. 4361-72, 2009.
- [13] I. Sechopoulos, D. R. Dance, J. M. Boone, H. T. Bosmans, M. Caballo, O. Diaz, R. van Engen, C. Fedon, S. J. Glick, A. M. Hernandez, M. L. Hill, K. W. Hulme, R. Longo, C. Rabin and W. B. Sanderink, "Joint AAPM Task Group 282/EFOMP Working Group Report: Breast dosimetry for standard and contrast-enhanced mammography and breast tomosynthesis," *Medical Physics*, vol 51, pp. 712-39, 2023.
- [14] A. Alsager, K. C. Young and J. M. Oduko, "Impact of heel effect and ROI size on the determination of contrast-to-noise ratio for digital mammography systems," *International Society for Optics and Photonics, Proc. SPIE 6913 Medical Imaging 2008: Physics of Medical Imaging*, article id. 69134I, 2008.
- [15] A. Hernandez, A. Seibert, A. Nosratieh and J. Boone, "Generation and analysis of clinically relevant breast imaging x-ray spectra," *Medical Physics*, vol. 44, no. 6, p. 148–2160, 2017.
- [16] M. Berger, J. Hubbell, S. Seltzer, J. Chang, J. Coursey, R. Sukumar, D. Zucker and K. Olsen, "XCOM: Photon Cross Sections Database (version 1.5)," November 2010. [Online]. Available: <https://www.nist.gov/pml/xcom-photon-cross-sections-database>.
- [17] R. van Engen, H. Bosmans, R. Bouwman, D. R. Dance, P. Heid, B. Lazzari, N. Marshall, N. Phelan, S. Schopphoven, C. Strudley, M. Thijssen and K. Young, "Protocol for the Quality Control of the Physical and Technical Aspects of Digital Breast Tomosynthesis Systems v1.03," European Commission, Luxembourg, 2013.

- [18] K. Young, J. Oduko, H. Bosmans, K. Nijs and L. Martinez, "Optimal beam quality selection in digital mammography," *British Journal of Radiology*, vol. 79, pp. 981-990, 2006.
- [19] K. Young, J. Cook and J. Oduko, "Automated and human determination of threshold contrast for digital mammography systems," In *Proceedings of the 8th International Workshop on Digital Mammography*, Berlin: Springer-Verlag, vol. 4046: 266-272, 2006.
- [20] K. Young, A. Alsager, J. Oduko, H. Bosmans, B. Verbrugge, T. Geertse and R. van Engen, "Evaluation of software for reading images of the CDMAM test object to assess digital mammography systems," *Medical Imaging 2008: Physics of Medical Imaging*, Proceedings of the SPIE, Volume 6913, article id. 69131C, 2008.
- [21] International Electrotechnical Commission, "IEC 62220-1-2: Determination of the detective quantum efficiency – Detectors used in mammography," International Electrotechnical Commission, Geneva, 2007.
- [22] J. Oduko, C. Strudley and K. Young, "Technical Evaluation of Siemens Inspiration PRIME with VB30L software," Public Health England, London, 2016.